Chapter 2
Shock Metamorphism of Terrestrial Impact Structures and its Application in the Earth and Planetary Sciences

Arnold Gucsik

2.1 Introduction

Shock metamorphism is the sum of irreversible chemical, mineralogical and physical changes in the target materials that occur during the hypervelocity impact event (Melosh 1989). The following chapters have been summarized from reviews by French and Short (1968); Sharpton and Grieve (1990); Stöffler and Langenhorst (1994); Grieve et al. (1996); Koeberl (1997) and French (1998).

When an extraterrestrial projectile (comet or asteroid) hits target rocks of a planetary surface, geologic materials are subjected to shock pressures above their Hugoniot Elastic Limit (HEL), which is on the order of 5-10 Gigapascals (GPa) (Sharpton and Grieve 1990). Shock metamorphism provides evidence for conditions associated with impact cratering (e.g., French and Short 1968; Stöffler and Langenhorst 1994; Grieve et al. 1996; Koeberl 1997; French 1998, Deutsch 1998 and references therein) including the high pressures, temperatures, and strain rates ($10^6 - 10^8$ s^{-1}), which lead to as characteristic structural and phase changes in minerals. Figure 2.1 shows that endogenic metamorphism of crustal rocks does not exceed temperatures of 1200°C and pressures of 2 GPa, except static pressure, which affects specific deep-seated rocks, as for example eclogites (Koeberl 1997).

Large impact events differ in many ways from endogenic processes such as volcanic explosions, earthquakes, and plate tectonics (French 1998):

- There have been no historical records or examples of large meteorite impacts.
- The impact energy is limited only by the mass and velocity of the projectile and concentrated within a fraction of time compared to the hundreds or thousands of years through volcanism, earthquakes, tectonic processes, and heat flow.
- The energy is released in an impact event shattering, deforming, melting, and even vaporising large volumes of target rock in a fraction of seconds.
- Large impact events cause biological extinctions, because their impact energy is released near the surface and directly into the biosphere.

Arnold Gucsik (✉)
Max Planck Institut für Chemie, Abteilung Geochemie, Joh.-J.-Becherweg 27. Universitätcampus, D-55128 Mainz, Germany
e-mail: gucsik@mpch-mainz.mpg.de

A. Gucsik (ed.), *Cathodoluminescence and its Application in the Planetary Sciences*,

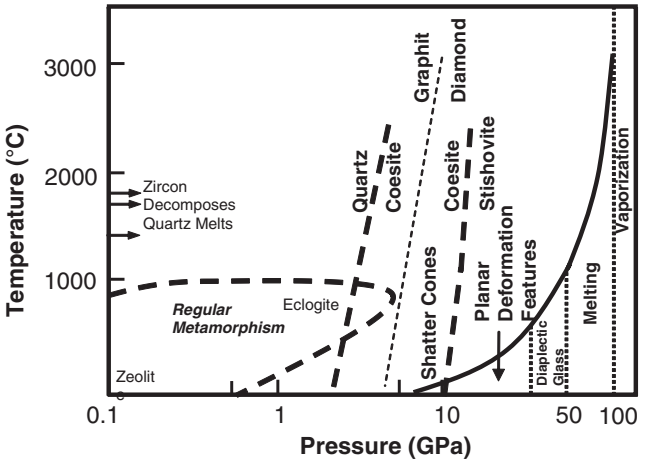

Fig. 2.1 Conditions of endogenic metamorphism and shock metamorphism in the pressure-temperature fields. This comparison diagram exhibits the onset pressures of various irreversible structural changes in the rocks due to shock metamorphism and the relationship between pressure and post-shock temperature for shock metamorphism of granitic rocks (modified after Koeberl 1997; his Fig. 2.2))

- Unique deformation effects occurred as changes in minerals such as mineral deformations and melting under the extreme high pressure and temperature (e.g., the shock pressure may be than 60 GPa and post-shock temperature may be 2000°C).

2.2 Impact Cratering Mechanics

The impact cratering process is commonly divided into the contact and compression, excavation, and modification stages (Gault et al. 1968; Melosh 1989 1992,). During the compression stage, structural modifications and phase changes occurred in the target rocks. The morphology of a crater is developed in the excavation and modification stages.

2.2.1 Contact and Compression Stage

During the contact and compression stage, the projectile or impacting object first hits the planet's surface (the target) and transfers its energy and momentum to the underlying rocks. The projectile traveling at a few kilometers per second produces large specific kinetic energy ($E = 1/2mv^2$, m = mass, v = velocity) (Melosh 1992). For instance, a stony meteorite of only 6 m diameter, colliding with the Earth at 20

km/s, releases as much energy [8.3×10^{23} Joules (J) or 20,000 tons (20 kT) of TNT] as an atomic bomb (French 1998). This stage lasts only a bit longer than the time required for the impacting object to travel its own diameter,

$$t_{cc} = L/v_i, \tag{2.1}$$

where t_{cc} is the duration of contact and compression, L the projectile diameter, and v_i the impact velocity.

The shock wave in the projectile reaches its back (or top) surface in contact and compression stage. Simultaneously, the pressure is released as the surface of the compressed projectile expands upward (wave of pressure relief propagates back downward toward the projectile-target interface). During the irreversible compression process, the projectile has been compressed to high pressure (hundreds of gigapascals) producing liquid or gaseous state due to heat deposited in the projectile (Melosh 1992).

Very high velocity jets of highly shocked material are formed, where strongly compressed material is close to a free surface. The jet velocity depends on the angle between the converging surface of the projectile and the target, but may exceed the impact velocity by factors as large as five (Melosh 1992).

2.2.1.1 Hugoniot Elastic Limit (HEL)

The projectile hits the target, generating strong shock waves, which leads to compression of the target rocks at pressures far above a material parameter called the Hugoniot elastic limit (Melosh 1989). The Hugoniot Elastic Limit (HEL) describes the maximum stress in an elastic wave that a material can be subjected to without permanent deformation (Melosh 1989). The value of the HEL is about $5-10$ GPa for most minerals and whole rocks. The only known natural process that generates these high shock pressures exceeding the HELs is hypervelocity impact. The strength of the shock waves can be demonstrated or measured from the Hugoniot equations, relating quantities in front of the shock wave (subscript 0) to quantities behind the shock wave (Melosh 1989)

$$\rho(U-\mu_p) = \rho_0 U \tag{2.2}$$

$$P - P_0 = \rho_0 \mu_p U \tag{2.3}$$

$$E - E_0 = 1/2(P+P_0)(1/\rho_0 - 1/\rho) \tag{2.4}$$

where P is pressure, ρ density, μ_p particle velocity after the shock, U the shock velocity, and E energy per unit mass. These three equations are equivalent to the conservation of mass, momentum, and energy, respectively, across the shock front. The Hugoniot equations must be supplemented by a fourth equation, the equation of state, that relates the pressure to the density and internal energy in each material,

$$P = P(\rho, E) \tag{2.5}$$

Alternatively, a relation between shock velocity and particle velocity may be specified,

$$U = U(\mu_p) \tag{2.6}$$

As this relation is frequently linear, it often provides the most convenient equation of state in impact processes. Thus, we can write:

$$U = c + S\mu_p \tag{2.7}$$

where c and S are empirical constants. These equations can be used to compute the maximum pressure, particle velocity, shock velocity, etc. in an impact (Melosh 1992). A Hugoniot equation of state curve is a shock wave equation of state data, which are plotted on a P-V plane (Fig. 2.2). It defines the locus of all shock states achievable in any material by shock waves of variable intensity, e.g., by various impact velocities of a projectile (Melosh 1989; Koeberl 1997).

Temperatures in the shocked states can be determined by integrating the following equation because of the internal energy, which is related to temperature and volume through an equation of state (Martinez et al. 1995; Martinez and Agrinier 1998):

$$\frac{dT}{dV} = T\left[\frac{\gamma}{V}\right] + \left[\frac{dP}{dV}(V_0 - V) + (P_0 - P)\right]\frac{1}{2C_v} \tag{2.8}$$

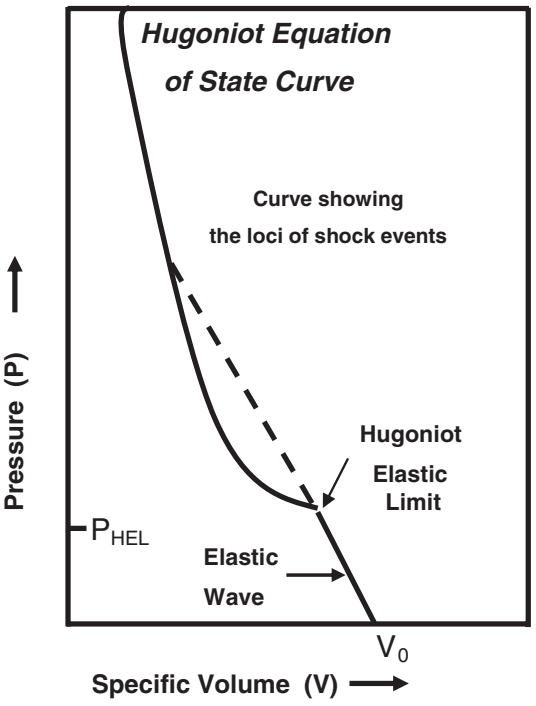

Fig. 2.2 The Hugoniot equation state curve does not represent a continuum of states as in thermodynamic diagrams, but the loci of individual shock compression events. The yielding of the material at the Hugoniot Elastic Limit is indicated (modified after Koeberl 1997; his Fig. 2.1)

where V_0 and P_0 are initial volume and pressure.

Models of specific heat C_v and Grüneisen parameters γ (which are quantities that are relatively constant by the product of three times the coefficient of linear expansion divided by the product the compressibility with the specific heat per unit volume) at high temperature and compression are therefore required for calculating shock temperatures (Melosh 1989; Martinez and Agrinier 1998).

Post-shock temperatures in the material can be related to temperatures in the shocked state using

$$\frac{dT}{dV} = -T\left[\frac{\gamma}{V}\right] \tag{2.9}$$

which is the adiabatic part of the Hugoniot equation and represents the adiabatic decompression from the shock state to the final zero-pressure state (Melosh 1989; Martinez and Agrinier 1998).

2.2.2 Excavation Stage

The expanding shock waves open the actual impact crater during the excavation stage (Melosh 1989; Grieve 1991). The transient cavity is a freshly opened bowl-shaped crater and surrounded by an ejecta curtain that develops is several orders of magnitude larger than the diameter of the projectile.

At the high pressures and post-shock temperatures the rocks may melt or even vaporise upon release. The lower pressures cause pervasive fracturing and planar deformation elements in individual crystals and produce characteristic cone-in-cone fractures called shatter cones. The target material strength and gravity become important near the end of excavation. This stage ends much longer than the contact and compression stage, requiring seconds or minutes to reach completion, depending upon the several factors as follows: crater size, direction of the impact, impact velocities, presence of a water table or layers of different strength, rock structure, joints, or initial topography in the target (Melosh 1992).

2.2.3 Modification Stage

The modification stage begins when the transient crater collapses under gravity, and elastic rebound of the underlying, compressed rock layers may also play a role. It was suggested from volume conservation that the crater collapse appears almost immediately after formation of the transient crater, which produces an increase of the original diameter of the crater by about 15%. During modification, loose debris slides down the steep interior walls of small craters, pooling on the floor of the final bowl-shaped depression (Melosh 1992). The normal geologic processes of gradation, isostatic adjustment, infilling by lavas, sediments, etc. on geologic time scales may eventually result in obscuration or even total obliteration of the crater (Melosh 1992).

2.3 Types of Terrestrial Impact Craters

The Earth Impact Database is a resource that has been assembled since 1985 by researchers at the Geological Survey of Canada (a division of Natural Resources, Canada). It has now been transferred to the Planetary and Space Science Centre at the University of New Brunswick, Department of Geology. Here, 175 impact structures (2008) were registered on the webpage: www.unb.ca/passc/ImpactDatabase/. These confirmed terrestrial impact craters (Fig. 2.3) have two basic morphological forms: simple and complex. The two forms differ only in the diameter range at which the transition from one form to another takes place. On the Earth, simple craters occur up to a diameter of 4 km in crystalline and 2 km in sedimentary target rocks (Dence 1972). Terrestrial craters with a diameter greater than 4 km show a complex form. Depending on their size, complex craters may be further subdivided into peak ring crater and multiring basins.

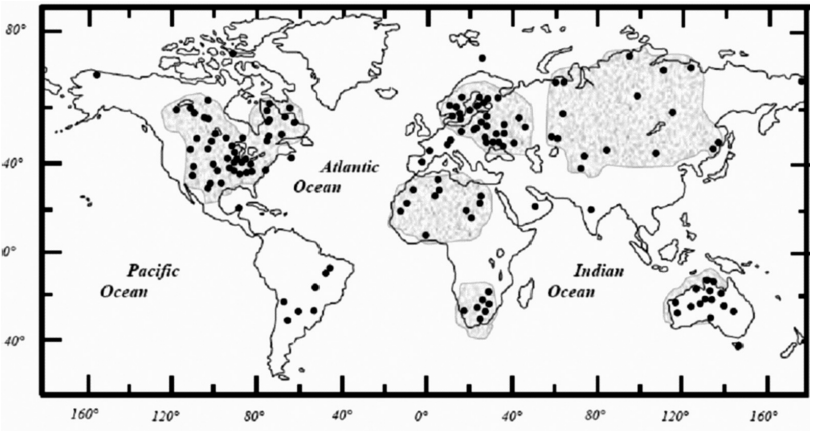

Fig. 2.3 Distribution of currently (2008) known impact structures, which are concentrated mainly to the cratonic areas (as indicated by grey regions) of continents (data from www.unb.ca/passc/Impact Database)

2.3.1 Simple Craters

Simple craters are the smallest impact structures and occur as bowl-shaped depressions (French 1998). These craters can be characterized by a structurally upraised and fractured rim area (e.g., Barringer Crater, Arizona, USA) (Fig. 2.4). The sizes of these craters are up to 2 km (sedimentary target rocks) to about 4 km in diameter (crystalline target rocks) on Earth, depending on the strength of the target rocks (Dence 1972; Melosh 1992). The interior of the crater has a smoothly sloping parabolic profile and its rim-to-floor depth is about one-fifth of its rim-to-rim diameter. The surrounding plain is blanketed with a mixture of ejecta (proximal ejecta)

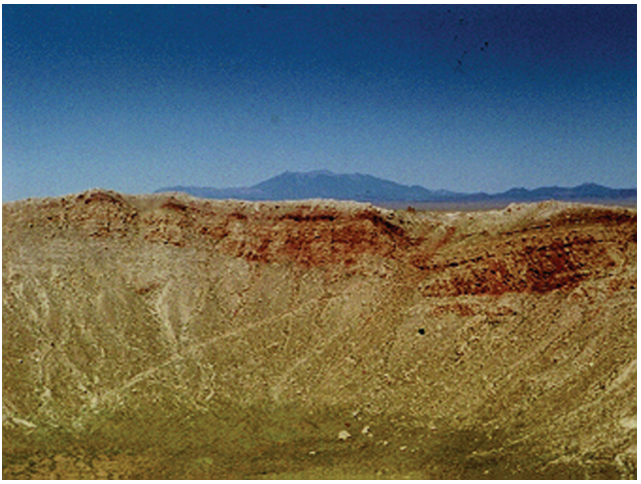

Fig. 2.4 A young, well-known and well-preserved simple impact crater (1.2 km in diameter): Barringer Meteor Crater (Arizona, USA). This crater was formed about 50.000 years ago, when an iron meteorite approximately 30 m across struck the horizontal sediments of northern Arizona's Colorado Plateau. The photo, looking northwest, shows the uplifted rim (photo by author)

and debris scoured from the pre-existing surface for a distance of about one crater diameter from the rim (Melosh 1992). The floor of simple craters is underlain by a lens of broken rock, breccia, which slid down the inner walls of the crater shortly following excavation. This breccia typically includes representatives from all the formations intersected by the crater and may contain layers of melted or highly shocked rocks.

2.3.2 Complex Craters

The complex craters have flat interior floors or internal rings instead of central peaks and formed with diameters larger than 4 km on Earth (depending on the target lithology). These craters are believed to have formed by collapse of an initially bowl-shaped transient crater, and because of this more complicated structure they are known as complex craters (Melosh 1992). The floors of complex craters are covered by melted and highly shocked debris. The surfaces of the terrace blocks tilt outward into the crater walls, and melt pools are also common in the depressions thus formed. The central peaks consist of material that is pushed upward from the deepest levels excavated by the crater. Complex craters are generally shallower than simple craters of equal size and their depth increases slowly with increasing crater diameter. Rim height also increases rather slowly with increasing diameter because much of the original rim slides into the crater bowl as the wall collapses (Melosh 1992). The amount of structural uplift (SU) at complex craters can be measured, where the subsurface stratigraphy is known. The relationship is:

$$SU = 0.06D^{1.1} \quad (2.10)$$

where SU is the amount of stratigraphic uplift undergone by the deepest lithology now exposed at the surface in the center and D is the diameter of the crater (Grieve 1991). The uplifted area may consist of parts of the upper crust at the larger complex craters (e.g., Siljan, SU = 4km; Manicouagan, SU = 9.5km). The ejecta blankets of complex craters show some similarities to those of simple craters. However, the hummocky texture characteristics of simple craters is replaced by more radial troughs and ridges as size increases (Melosh 1992).

2.4 Geology: Lithological Indicators of Impact Structures

An impact event is a surface process that produces circular, shallow, rootless structures in contrast to volcanic processes (French 1998). The lithological indicators for an impact structure may be a layer of fragmental breccia, which is found as crater filling or overlying a possibly raised, partially brecciated, and up- or over-turned rim (Koeberl 1997).

2.4.1 Breccia Types at Impact Structures

The impact-derived breccias contain shocked minerals, impact melts, and impact glasses in an impact crater (Stöffler and Langenhorst 1994; Koeberl 1997). The monomict and polymict breccias that formed during impact processes could be divided into three main types: (1) cataclastic (fragmental breccias), (2) suevitic (fragmental with a melt fragment component) breccias (Fig. 2.5a,b), or (3) impact melt (melt breccia - i.e., melt in the matrix with a clastic component) breccias. The

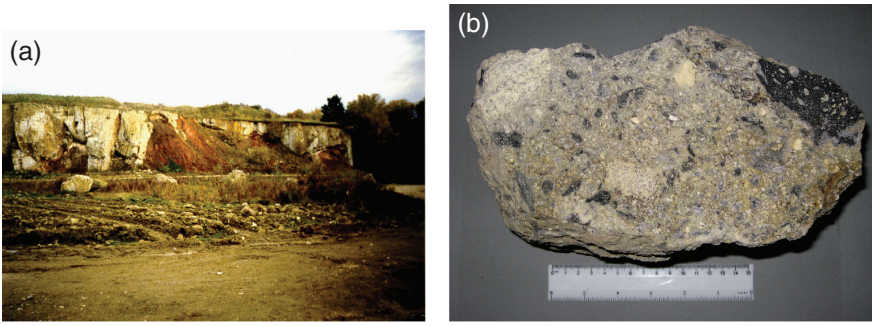

Fig. 2.5 (**a**) Aumühle quarry of suevite, which is located in the northwest of the Ries impact structure (Germany). This image shows a dark Jurassic clay and red clay and sandstones of the Keuperian. (**b**) Suevite: the elongated, grey parts of suevite are impact glasses (photos by author)

breccias can be allochthonous or autochthonous. Additionally, the basement rocks contain dikes of injected or locally formed fragmental or pseudotachylitic breccias (Reimold 1995). Whether all these breccia types are actually present at an impact crater depends on factors including the size of the crater, the composition of the target area (e.g., Kieffer and Simonds 1980), and the level of erosion (see; Horz 1982; Grieve 1987, and references therein).

2.4.2 Complete Melting

The target rocks undergo complete (bulk) melting to form impact melts at pressures in excess of about 60 GPa. The resulting melts are deposited as splash-form glass particles and "bombs" in suevitic breccias or as coherent impact melt body. The presence of inclusions of minerals, such as lechatelierite (monomineralic quartz melt that forms from pure quartz at temperatures at 1700°C), or baddeleyite (thermal decomposition product of zircon forming at a temperature of at least 1680°C), is associated with very high temperatures. Lechatelierite as a good indicator of meteorite impact origin is not found in any other natural rock, except in fulgurites, which form by fusion of soil or sand when lightning hits the ground (Stöffler and Langenhorst 1994; and references therein).

2.4.2.1 Impact Glasses

Impact glasses are more commonly found at relatively young impact craters rather than at old impact structures, because glass is not stable over geological times. Such impact-derived glasses have chemical and isotopic compositions that are similar to those of the target rocks. The similarities in chemical and isotopic composition between impactites and crater target rocks have been employed in several source crater investigations (e.g., Blum et al. 1993; Meisel et al. 1995). Impact glasses have much lower water contents (about 0.001-0.05 wt%) than volcanic or other natural glasses (Koeberl 1992). These impact melts and glasses are useful for the dating of an impact structure using K-Ar, ^{40} Ar$-^{39}$Ar, fission track, Rb-Sr, Sm-Nd, or U-Th-Pb isotope age-dating methods (Montanari and Koeberl 2000). The age that should be obtained for an impact event is different from that of volcanism because impact melts or glasses give a unique (local), much younger age as compared to the target rocks, which are usually old crustal rocks.

2.4.2.2 Tektites and Microtektites

The centimeter-sized tektites as chemically homogeneous glasses have been ejected from a few terrestrial impact structures and spread over thousands of kilometers. They found on land and have been subdivided into three groups: (a) normal or

splash-form tektites, (b) aerodynamically shaped tektites, and (c) Muong Nong-type tektites (or layered tektites). Tektites can be associated with smaller (≤ 1 mm) microtektekties (Montanari and Koeberl 2000).

Currently, on the basis of differences in location, age, and to some extent, the characteristics of tektites and microtektites, four strewn fields are known: (1) Australasian (0.78 Ma, source crater no yet identified); (2) Central European (15 Ma) from the Ries Crater, Germany; (3) Ivory Coast (1.07 Ma) from the Bosumtwi Crater, Ghana (Koeberl et al. 1997a); and (4) North American (35 Ma) from the Chesapeake Bay impact structure, USA (Fig. 2.6).

Tektites are formed as the product of melting and quenching of terrestrial rocks during hypervelocity impact on the Earth (see Montanari and Koeberl 2000), for a recent review). Their chemical and isotopic compositions are identical with those of the target rocks where the impact occurred:

- Typically high in silica composition (> 65 wt%), but their chemical and isotopic compositions are not volcanic, but closer to those of shales and similar sedimentary rocks. Containing low water content (≤ 0.02 wt%), and their flow-banded structure includes particles and bands of lechatelierite (monomineralic quartz melt).
- A few tektites contain partly melted inclusions of shocked and unshocked mineral grains (quartz, apatite, zircon) as well as coesite (Glass and Barlow 1979).

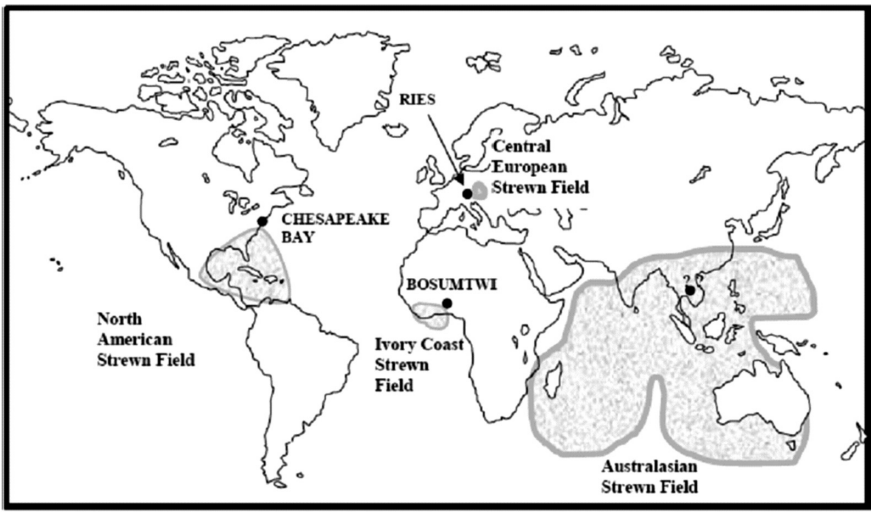

Fig. 2.6 Location (*solid circles*) known source craters (Chesapeake Bay, Ries, and Bosumtwi craters) and extension of the four tektite strewn fields. (modified after Montanari and Koeberl 2000; their Fig. 2.4.1.1

2.5 Diagnostic Shock Features in Impact Craters

The best diagnostic indicators for shock metamorphism are features that can be studied easily by using the polarizing microscope. They include planar microdeformation features; optical mosaicism; changes in refractive index, birefringence and optical axis angle; isotropization; and phase changes (Stöffler 1972, 1974; Stöffler and Langenhorst 1994; Grieve et al. 1996; Koeberl 1997).

2.5.1 Shatter Cones

Shatter cones (Fig. 2.7) are regarded as the only distinctive and unique shock deformation feature that develops on a macroscopic scale as hand specimen (Dietz 1968; French 1998). They are distinctive conical fractures produced in target rocks by shock waves of relatively low intensity, usually below the crater floor or in the central uplifts of large structures. They form in all kinds of target rocks subjected to the appropriate pressures, but they are most strikingly developed in fine-grained rocks, especially carbonates. Shatter cones can be distinguished from similar deformation features by the distinctive radiating striations (”horsetailing”) along the cone surface, and by the fact that the cones originally point in the direction of the source of the shock wave, i.e., inward and upward. They develop in a large volume of target rock and have been widely used to identify terrestrial impact structure. Shatter cones are good diagnostic structural criteria that are easy to recognize and are found in many terrestrial impact structures.

Fig. 2.7 Well-developed finely sculptured shatter cone, in fine-grained Ordovician limestone from the Charlevoix impact crater, Canada (photo by author)

The formation mechanism for shatter cones is poorly understood. The conical shapes might be related to the interactions of shock waves with point inhomogeneites in rocks, or interactions between the main compressive shock and rebound waves (Gash 1971). However, these models do not explain the dominant features of shatter cones such as characteristic striations, the ”horse-tail” cone hierarchy, and the variety of complete cones. More recently, Shagy et al. (2002) have shown that the shatter cones are branched tensile fractures. Shatter-cone striations are the preserved tracks of fracture front waves. Their analysis of the striations shows that shatter cones develop only at extreme propagation velocities, between $0.9V_R$ and the maximal permitted velocity of V_R. The angles of the striations (α), which are shown to increase systematically with the distance from the impact, reflect both the stresses and the energy flux driving the fracture at a given site, and may be used as a general tool to evaluate extreme local stresses in the field (Shagy et al. 2002).

2.5.2 Mosaicism

The term mosaicism describes the internal fragmentation of a single crystal into a mosaic of slightly disoriented crystal domains. Mosaicism is a microscopic expression of shock metamorphism observed in a number of rock-forming minerals (see, e.g., Horz and Quaide 1973) and appears as an irregular, mottled optical extinction pattern. This is distinctly different from the undulatory extinction that occurs in tectonically deformed quartz and, generally, accompanied in many minerals by indications of plastic deformation structures or deformation bands (Stöffler 1972). Mosaicism can be semi-quantitatively investigated by X-ray diffraction.

2.5.3 Kink Bands

Kink bands appear in sheet silicates, other sheet-like structures in shocked quartz and feldspar (Bunch 1968). They are not oriented parallel to rational crystallographic planes and display variable disorientation with respect to the host lattice compared to the deformation twins. Kink banding is considered as supporting evidence for the impact origin of a structure, but it cannot be used as a single diagnostic criterion, as it occurs also in metamorphic rocks.

2.5.4 Planar Microstructures

Two types of planar microstructures are apparent in shocked minerals: planar fractures (PFs) and planar deformation features (PDFs). Their essential characteristics are summarized in Table 2.1. The PDFs occur as either non-decorated or decorated

Table 2.1 Characteristics of planar fractures and planar deformation feature in quartz

Nomenclature	1. Planar fractures (PF) 2. Planar deformation features (PDF) 2.1. Nondecorated PDFs 2.2. Decorated PDFs
Crystallographic orientation	1. PFs: usually parallel to (0001) and $\{10\bar{1}1\}$ 2. PDFs: usually parallel to $\{10\bar{1}3\}$,$\{10\bar{1}2\}$, $\{10\bar{1}1\}$, (0001), $\{11\bar{2}2\}$, $\{11\bar{2}1\}$, $\{10\bar{1}0\}$,$\{11\bar{2}0\}$, $\{21\bar{3}1\}$, $\{51\bar{6}1\}$, etc.
Optical microscope properties	Multiple sets of PFs or PDFs Thickness of PDFs: $< 2-3\mu m$ Spacing: >15 μm (PFs), 2-10 μm (PDFs)
TEM properties (PDFs)	Two types of primary lamellae are observed: 1. Amorphous lamellae with a thickness of about 30 nm (pressures of <25 GPa) and about 200 nm (at pressures of >25 GPa) 2. Brazil twin lamellae parallel to (0001)

Data from Stöffler and Langenhorst (1994).

PDFs (Stöffler and Langenhorst 1994). Planar deformation features in rock-forming minerals (e.g., quartz, feldspar, or olivine) are generally accepted to provide diagnostic evidence for shock deformation (see, e.g., French and Short 1968; Stöffler and Langenhorst 1994; Grieve et al. 1996; French 1998, and references therein).

2.5.4.1 Planar Fractures (PFs)

Planar fractures are parallel sets of multiple planar cracks or cleavages in quartz grains; they develop at the lowest pressures characteristic of shock waves ($\sim 5-8$ GPa) (French 1998). As French (1998) noted, they are parallel to rational crystallographic planes with low Miller indices, such as (0001) and $\{101\}$. The fractures are typically $5-10\mu m$ wide and spaced $15-20\mu m$ or more apart in individual quartz grains. Similar cleavage occurs also rarely in quartz from non-impact settings, and therefore planar fractures cannot be used independently as a single criterion for meteorite impact. However, the development of intense, widespread, and closely spaced planar fractures are frequently accompanied in impact structures by other features clearly formed at higher shock pressures (French 1998, and references therein). Planar deformation features, together with the somewhat less specific planar fractures (PFs), are usually well developed in quartz (Stöffler and Langenhorst 1994).

2.5.4.2 Planar Deformation Features (PDFs)

PDFs in various minerals (especially in quartz) have long been known as evidence of impact-induced deformation. In contrast to planar fractures, PDFs are not open cracks. They occur as multiple sets of more closely spaced (typically $2-10\mu m$), narrow (typically $< 2-3\mu m$), parallel planar regions than planar fractures. PDFs occur in planes corresponding to specific rational crystallographic orientations. The basal (0001) or c, $\{10\bar{1}3\}$ or ω, and $\{10\bar{1}2\}$ or π, orientations are the most common planes in quartz. In addition, PDFs often occur in more than one crystallographic orientation per grain. At pressures about ≥ 35 GPa, the distances between the planes decrease, and the PDFs become more closely spaced and more homogeneously distributed over the grain. Depending on the peak pressure, PDFs are observed in $2-10$ (maximum 18) orientations per grain (Robertson et al. 1968; Stöffler 1972; Stöffler and Langenhorst 1994; Grieve et al. 1996; Koeberl 1997). To properly characterize PDFs, it is necessary to measure their crystallographic orientations optically by using either a universal stage (Emmons 1943) or a spindle stage (Medenbach 1985), or by transmission electron microscopy (see, e.g., Goltrant et al. 1991; Leroux et al. 1994).

The formation mechanisms of these features in naturally shocked quartz might be explained by the pressure dependence of the shear modulus (decreasing linearly with increasing pressure and, for some planes even discontinuously, for a critical pressure of the order of 10 GPa) of quartz for various planes and directions. The Si-O-Si bonds are more easily broken, allowing the corresponding atoms to move towards energetically more favourable positions. This progressive reorganization leads to the formation of a new structure (dense amorphous silica lamellae). The transformation occurs very rapidly, as it is driven by the front of the shock wave. This explanation predicts that the density of PDFs should markedly increase with shock intensity (Goltrant et al. 1992).

2.5.5 Diaplectic Glass

Diaplectic glass is formed at shock pressures in excess of about 35 GPa without melting by solid-state transformation and has been described as a phase intermediate between crystalline and normal glassy phases (Stöffler and Hornemann 1972). It is found at numerous impact craters and shows the original crystal defects, planar features, and absence of flow structures and vesicles. Maskelynite is a diaplectic plagioclase glass formed in a similar way and at similar pressure range as diaplectic quartz glass. Diaplectic glass has a refractive index that is slightly lower than that of synthetic quartz glass. Other minerals (mafics) tend to oxidize or decompose.

2.5.6 Lechatelierite

At pressures that exceed about 50 GPa, lechatelierite forms by fusion of quartz. In contrast to diaplectic glass, lechatelierite is formed by a liquid state transformation associated with the melting of quartz at higher temperatures ($> 1700°C$) than occur in volcanic processes. This is a good indicator of a meteorite impact origin. Other minerals also melt at sufficiently high temperatures, e.g., feldspar (Stöffler and Langenhorst 1994).

2.5.7 High-Pressure Polymorphs

The high-pressure SiO_2polymorphs, coesite (pressure range: $30-60$ GPa) and stishovite (pressure range: $12-45$ GPa), occur as very fine-grained aggregates that are formed by partial transformation of the host quartz during shock metamorphism (Grieve et al. 1996). Under conditions of static equilibrium, where reaction rates are slower and kinetic factors less important, coesite forms from quartz at lower pressures (> 2 GPa) than does stishovite ($10-15$ GPa) (French 1998). The identification of coesite and stishovite at several impact sites in the early 1960s provided one of the earliest criteria for establishing the impact origin of several structures, most notably the Ries crater, Germany (Chao et al. 1960; Shoemaker and Chao 1961), and the Bosumtwi crater (Littler et al. 1961). Impact-derived coesite occurs as very fine-grained, colorless to brownish, polycrystalline aggregates, up to $100-200\mu m$ in size, usually embedded in diaplectic quartz glass, or rarely, in nearly isotropic quartz with abundant planar deformation features and a mean refractive index below 1.48 (Stöffler and Langenhorst 1994). Coesite occurs also in metamorphic rocks of ultra-high pressure origin or in kimberlites.

Other high-pressure mineral phases include jadeite formed from plagioclase, majorite from pyroxene, and ringwoodite from olivine (Stöffler 1972). Impact derived diamonds (the high-pressure cubic modification of carbon) have also been found at various craters. These diamonds form from carbon in the target rocks, mainly in graphite-bearing (e.g., graphitic gneiss) or coal-bearing rocks (Koeberl et al. 1997b).

2.6 Cathodoluminescence Properties of the Shocked Minerals

2.6.1 Quartz

The CL luminescence emission in the unshocked quartz might be associated with defect structures. The silicon dioxide structure is modified by different types of defect structures (impurities, vacancies, etc), which occur in the short range order. Hence, similar types of defects are found in crystalline and amorphous polymorphs of silicon dioxide (Kalceff et al. 2000-and references therein). Generally, the lu-

minescence of quartz shows different CL colors depending on its origin. Previous work on CL properties of shocked quartz is limited. Owen and Anders (1988), in a pioneering study, showed that quartz from intrusive igneous and high-grade metamorphic rock shows darker purple-blue CL, whereas quartz from low-grade metamorphic rocks exhibit reddish-brown CL, and that shocked quartz from the Cretaceous-Tertiary (K/T) boundary exhibits CL colors similar to those of low-grade metamorphic quartz. Owen and Anders (1988) used these observations to demonstrate that shocked quartz from the K-T boundary was not derived from volcanic sources. At that time (1988), this was an important contribution to the study of the then controversial origin of the K-T boundary. Ramseyer et al. (1992) reported CL luminescence changes for quartz and feldspar from the granitic rocks of the Siljan impact structure, Sweden, and related their findings to complex alteration of the minerals during a post-impact hydrothermal overprint. Seyedolali et al. 1997) reported CL studies of shocked quartz grains from the Mjølnir impact structure (Barents Sea) in comparison with quartz from a variety of other sources. These authors studied patterns of variable-intensity CL, including zoning, healed fractures, complex fractures, complex shears and planar microdeformations from different source rocks, using a combined scanning electron microscopy (SEM)-CL fabric-analysis technique. Recently, Boggs et al. (2001) studied planar deformation features (PDFs) in shocked quartz from the Ries crater, Germany, using a SEM-CL imaging facility. He found that (in contrast to planar microstructures associated with tectonic fracturing) these features are filled by amorphous silica and appear as dark lines in the CL images, which indicate absence of recombination centers to the emission of photons. More recently, Gucsik et al. (2004a) described that cathodoluminescence spectra of unshocked and experimentally shock-deformed quartzite samples show broad bands in the near-ultraviolet range and the visible light range, at all shock pressures. These broad bands might be associated with defect centers on, e.g., SiO_4 groups. There are distinct differences between the CL spectra of the unshocked and the shocked samples, and shifts in the center positions of the broad bands are evident with increasing shock pressure. This might indicate that recombination centers or traps for the photon emission are more closely-spaced in the band gap between VB and CB as a function of the increasing shock pressure, which is probably caused by partial amorphization.

2.6.2 Feldspars

Sippel and Spencer (1970) observed that the shock metamorphism caused peak shifts from green peak toward the red peak, peak broadening and decrease of luminescence intensity than in the undamaged counterpart in the CL spectra of shock-metamorphosed lunar feldspars. They noted that the distortions or disorder in the crystal field results in crystal field perturbations and these local variations occur broadened distribution of excited state energies. More recently, CL spectral measurements were performed on natural and experimentally shocked

oligoclases (An19.7 single crystal shocked between 10.5 and 45 GPa) and plagioclases from the equilibrated ordinary chondrites (Dar al Gani, Tenham) (Kaus and Bischoff (2000,). They observed disappearance of the crystal field sensitive Mn^{2+} and Fe^{3+}-related peaks resulting from breakdown of the crystal structure (i.e., occurrence of diaplectic glass) at around 35 GPa.

2.6.3 Zircon

Thorough understanding of the shock metamorphic signatures of zircon will provide a basis for the application of this mineral as a powerful tool for the study or recognition of old, deeply eroded, and metamorphically overprinted impact structures and formations.

According to Gucsik et al. (2004b and references therein) the unshocked samples show crosscutting, irregular fractures in the images. The 38 GPa sample exhibits a dense pattern of narrow-spaced lamellar features, in CL mode, that could represent the twinning effect noted in a 40 GPa sample by earlier workers and which was ascribed to partial conversion from the zircon phase to the more voluminous scheelite-structure phase. The CL images of experimentally, at 40, 60, and 80 GPa, shocked samples show subplanar and nearly parallel microdeformations. All experimentally shocked zircon, as well as all investigated naturally shocked samples from the Ries crater, shows an inverse relationship between the brightness of the backscattered electron (BSE) signal and the corresponding cathodoluminescence intensity of the zonation patterns. The CL spectra of unshocked and experimentally shock-deformed specimens and naturally shock-metamorphosed zircon samples are characterised by narrow emission lines and broad bands in the region of visible light and in the near-ultraviolet range. The emission lines result from rare earth element activators and the broad bands might be associated with lattice defects.

2.6.4 Impact-Derived Glasses

According to Gucsik et al. (2003 and references therein) CL images of the Aouelloul impact glass, Muong Nong-type tektite, and Libyan Desert Glass samples show more variety than the BSE images. In all three cases are brightness and contrast variations inversely correlated between the BSE and the CL images, and features that appear in the BSE image can usually also be discerned in the CL image. In fact, the CL images show more pronounced contrast and brightness variations than the BSE images. The CL images seem to preserve target rock textures much better than any other electron image, even though the samples appear to be totally glassy. The Aouelloul sample shows quite clearly a granular structur, which might be related to the texture of the original sandstone. Most spectacular are the CL images of the Libyan Desert Glass, which show a distorted original texture, probably indi-

cating high-temperature glass flow, which is not apparent at all in the BSE images. The inverse relationship between BSE and CL brightness might be caused by high concentrations of Al, Li and Na, which can lead to quenching of the CL signal.

Broad bands in the CL spectrum indicate that excited and ground states of the electronic radiative transitions are strongly coupled with the vibrating lattice. Stronger coupling indicates that more phonons are emitted in the electronic transition. (1) Broad intrinsic emission generally results from self trapped exciton (STE) which are highly localised excitons trapped by their own self-induced lattice distortion. The emission energy of the STE is usually much lower than the band gap of the material due to the energy lost by phonon emission during the electronic transition. (2) Excitation of electrons or holes trapped (dangling bonds in covalent crystals) at point defects such as vacancies, interstitial and point defect clusters usually produce broad CL peaks at all temperatures.

According to Stevens Kalceff et al. (2000, and references therein) the normal defect free configuration of (low pressure) silicon dioxide polymorphs can be represented as ($\equiv \mathrm{Si} - \mathrm{O} - \mathrm{Si} \equiv$) indicating that each silicon atom is surrounded by four tetrahedrally configured oxygen atoms and the adjacent silicon atoms are bridge bonded through a single oxygen atom. The silicon dioxide structure may be modified by the presence of defects (e.g., impurities, vacancies, etc.). The detected luminescence bands of the crystalline and amorphous modifications of SiO_2 are attributed to three optical active luminescence centers: (1) two-fold coordinated silicon (=Si:), non-bridging oxygen hole centre (NBOHC) and the self trapped exciton (STE). They found a red band at 650 nm due to a band-band recombination centre, a blue at 460 nm triplet-singlet and an ultraviolet at 290 nm singlet-singlet defect luminescence band.

- Thus, the two broad bands observed at 332 (3.73 eV) and around 440 (2.79 eV) nm in the cathodoluminescence spectra of Aouelloul impact glass and Muong Nong-type tektite might be related to the presence of such defect centers. The broad band at 332 nm (3.73 eV) might be attributed to the dominant defects, which occur in the short range order involving the slightly distorted SiO_4 tetrahedra. These defects are common to both the crystalline and amorphous SiO_2 structures. The band at 444 nm (2.79 eV) is probably associated with the radiative relaxation of the STE in quartz, which is strongly polarized along the c-axis (Kalceff et al. 2000). The broad band at 390 nm (3.17 eV) in the cathodoluminescence spectrum of the Libyan Desert Glass might be related to defect centers in the SiO_2 structure (e.g., $-\mathrm{O} - \mathrm{O}-;\mathrm{O}_2$) (Stevens Kalceff et al. 2000). The CL images of the tektite show only a few areas with brightness variations, whereas the Aouelloul glass and the Libyan Desert Glass CL images show significant variations in contrast and brightness.

References

Blum JD, Chamberlain CP, Hingston MP, Koeberl C, Marin LE, Schuraytz BC, Sharpton VL (1993) Isotopic comparison of K-T boundary impact glass with melt rock from the Chicxulub and Manson impact structures. Nature 364:325-327

Boggs S, Krinsley DH, Goles GG, Seyedolali A, Dypvik H (2001) Identification of shocked quartz by scanning cathodoluminescence imaging, Meteorit Planet Sci 36: 783-793

Bunch TE (1968) Some characteristics of selected minerals from craters. In: French BM, Short NM (eds) Shock metamorphism of natural materials. Mono Book Corporation, Baltimore, 413-432 pp.

Chao ECT, Shoemaker EM, Madsen BM (1960) First natural occurrence of coesite. Science 132: 220-222

Dence MR (1972) The nature and significance of terrestrial impact structures. 24th International Geological Congress, Montreal, Canada. Proceedings Section 15: 77-89

Deutsch A (1998) Examples for terrestrial impact structures. In: Marfunin, S.A. (ed), Mineral matter in space, mantle, ocean floor, biosphere, environmental management, and jewelry. Adv Min vol. 3, Springer-Verlag, Berlin, Heidelberg, pp 119-129

Dietz RS (1968) Shatter cones in cryptoexplosion structures. In: French MB, Short NM (Eds.) Shock metamorphism of natural materials. Mono Book Corporation, Baltimore 267-285 pp.

Emmons RC (1943) The Universal Stage (With Five Axes of Rotation). Geol Soc Am Memoir 8:205 pp.

French BM (1998) Traces of Catastrophe: A Handbook of Shock-Metamorphic Effects in Terrestrial Meteorite Impact Structures. LPI Contribution No. 954, Lunar and Planetary Institute, Houston, 120 pp.

French BM, Short NM, (Eds) (1968) Shock metamorphism of natural materials. Mono Book Corporation, Baltimore, 644 pp.

Gault DE, Quaide WL, Oberbeck VR (1968) Impact cratering mechanics and structures. In: French BM, Short NM (Eds.), Shock metamorphism of natural materials. Mono Book Corporation, Baltimore, pp. 87-99.

Gash PFJ (1971) Dynamic mechanism for the formation of shatter cones. Nature 230:32-35

Glass BP, Barlow RA (1979) Mineral inclusions in Muong Nong-type indochinites: Implications concerning parent material and process of formation. Meteoritics 14:55-67

Goltrant O, Cordier P, Doukhan JC (1991) Planar deformation features in shocked quartz: a transmission electron microscopy investigation. Earth Planet Sci Lett 106:103-115

Goltrant O, Leroux H, Doukhan J-C, Cordier P. (1992) Formation mechanism of planar deformation features in naturally shocked quartz. Phys Earth Planet Inter 74:219-240

Gucsik A, Koeberl Ch, Brandstätter F, Libowitzky E, Ming, Z. (2004a) Infrared, Raman, and cathodoluminescence studies of impact glasses. Meteoritics and Planetary Science 39: 1273-1285

Gucsik A, Koeberl C, Brandstätter F, Libowitzky E Reimold WU (2004b) Cathodoluminescence, electron microscopy, and Raman spectroscopy of experimentally shock metamorphosed zircon crystals and naturally shocked zircon from the Ries impact crater. In: Dypvik H, Burchell M, Claeys Ph, (eds.) Cratering in Marine Environments and on Ice, Springer-Verlag, Heidelberg, pp 281-322.

Gucsik A, Koeberl Ch, Brandstätter F, Libowitzky, E, Reimold, WU (2003) Scanning electron microscopy, cathodoluminescence, and Raman spectroscopy of experimentally shock-metamorphosed quartzite. Meteorit Planet Sci 38:1187-1197

Grieve RAF (1987) Terrestrial impact structures. Annu Rev Earth Planet Sci 15:245-270

Grieve RAF (1991) Terrestrial impact: The record in the rocks. Meteoritics 26: 175-194

Grieve RAF, Langenhorst F, Stöffler D. (1996) Shock metamorphism of quartz in nature and experiment: II. Significance in geoscience. Meteorit Planet Sci 31:6-35

Hörz F (1982) Ejecta of the Ries crater, Germany. In: Silver LT, Schultz PH (eds.), Geological implications of impacts of large asteroids and comets on the Earth. Geol Soc Am Spec Paper 190: 39-55

Hörz F, Quaide WL (1973) Debye-Scherrer investigations of experimentally shocked silicates. Moon 6: 45-82

Kaus A, Bischoff A, (2000) Cathodoluminescence (CL) properties of shocked plagioclase, Meteorit Planet Sci 35:A 86

Kieffer SW, Simonds CH (1980) The role of volatiles and lithology in the impact cratering process. Rev Geophys Space Phys 18:143-181

Koeberl C (1992) Water content of glasses from the K/T boundary, Haiti: indicative of impact origin. Geochim Cosmochim Acta 56:4329-4332

Koeberl C (1997) Impact cratering: the mineralogical and geochemical evidence. In: Johnson KS, Campbell JA (eds) Ames structure in northwest Oklahoma and similar features: origin and petroleum production (1995 symposium). Okl Geol Surv Circ 100: 30-54

Koeberl C, Bottomley R, Glass BP, Storzer D (1997a) Geochemistry and age of Ivory Coast tektites and microtektites. Geochim Cosmochim Acta 61: 1745-1772

Koeberl C, Masaitis VL, Shafranovsky GI, Gilmour I, Langenhorst F, Schrauder M (1997b) Diamonds from the Popigai impact structure, Russia. Geology 25:967-970

Leroux H, Reimold WU, Doukhan J-C (1994) A T.E.M. investigation of shock metamorphism in quartz from the Vredefort dome, South Africa. Tectonophysics 230:223-239

Littler J Fahey JJ Dietz RS Chao ECT (1961) Coesite from the Lake Bosumtwi crater, Ashanti, Ghana. Geol Soc Am Spec Paper 68:218

Martinez I, Agrinier P (1998) Meteorite impact craters on Earth: major shock induced effects in rocks and minerals. Earth Planet Sci 327:75-86

Martinez I, Deutsch A, Schärer U, Ildefonse P, Guyot F, Agrinier P. (1995) Shock recovery experiments on dolomite and thermodynamical calculations of impact induced decarbonation. J Geophys Res 100:15,465-15,476

Medenbach O (1985) A new microrefractometer spindle stage and its application. Fortsch Mineral 63: 111-133

Meisel T, Krähenbühl U, Nazarov MA (1995) Combined osmium and strontium isotopic study of the Cretaceous-Tertiary boundary at Sumbar, Turkmenistan: A test for an impact vs. volcanic hypothesis. Geology 23:313-316

Melosh HJ (1989) Impact Cratering: A geologic process. Oxford University Press, New York, 245 pp.

Melosh HJ (1992) Impact crater geology. In: Nierenberg WA (Ed.), Encyclopedia of earth system science 2. Academic Press, San Diego, pp 591-605.

Montanari A, Koeberl C (2000) Impact stratigraphy: The italian record. Lecture Notes in Earth Sciences 93, Springer, Heidelberg, 364 pp.

Owen MR, Anders HM (1988) Evidence from cathodoluminescence from non-volcanic origin of shocked quartz at the Cretaceous/Tertiary boundary, Nature 334:145-147

Ramseyer K, AlDahan AA, Collini B, Lindström O (1992) Petrological modifications in granitic rocks from the Siljan impact structure: evidence from cathodoluminescence. Tectonophysics 216:195-204

Reimold WU (1995) Pseudotachylite in impact structures - generation by friction melting and shock brecciation?: A review and discussion. Earth Sci Rev 39: 247-265

Robertson PB, Dence MR, Vos MA (1968) Deformation in rock-forming minerals from Canadian craters. In: French BM, Short NM, (Eds.) Shock metamorphism of natural materials. Mono Book Corporation, Baltimore, pp. 433-452.

Seyedolali A, Krinsley DH, Boggs S, O'Hara PF, Dypvik H, Goles G (1997) Provenance interpretation of quartz by scanning electron microscope-cathodoluminescence fabric analysis, Geology 25:787-790

Shagy A, Reches Z, Fineberg J, (2002) Dynamic fracture by large extraterrestrial impacts as the origin of shatter cones. Nature 418: 310-313

Sharpton VL, Grieve RAF (1990) Meteorite impact, cryptoexplosion, and shock metamorphism; A perspective on the evidence at the K/T boundary. Geol Soc Am Spec Paper 247: 301-318
Shoemaker EM, Chao ECT (1961) New evidence for the impact origin of the Ries Basin, Bavaria, Germany. J Geophys Res 66: 3371-3378
Sippel RF, Spencer AB (1970) Luminescence petrography and properties of lunar crystalline rocks and breccias, Proc. Apollo 11 Lunar Sci.Conf. 3:2413-2426
Kalceff MAS, Phillips MR, Moon AR, Kalceff W (2000) Cathodoluminescence microcharacterisation of silicon dioxide polymorphs: In: Pagel M, Barbin V, Blanc Ph, Ohnenstetter D (eds) Cathodoluminescence in Geosciences. Springer, Heidelberg, p. 193-224
Stöffler D (1972) Deformation and transformation of rock-forming minerals by natural and experimental shock processes: I. Behaviour of minerals under shock compression. Fortsch Mineral 49: 50-113
Stöffler D (1974) Deformation and transformation of rock-forming minerals by natural and experimental processes: II. Physical properties of shocked minerals. Fortsch Mineral 51: 256-289
Stöffler D, Grieve RAF (1994) Classification and nomenclature of impact metamorphic rocks. 25th Lunar and Planetary Science Conference 1347-1348
Stöffler D, Langenhorst F (1994) Shock metamorphism of quartz in nature and experiment: I. Basic observation and theory. Meteoritics 29:155-181
Stöffler D, Hornemann U (1972) Quartz and feldspar glasses produced by natural and experimental shock. Meteoritics 7:371-394

http://www.springer.com/978-3-540-87528-4

Cathodoluminescence and its Application in the Planetary Sciences

Gucsik, A. (Ed.)

2009, XII, 160 p. 66 illus., 34 illus. in color., Hardcover
ISBN: 978-3-540-87528-4